2014-01-01

Modeling Tidally Driven Coulomb Failure At Strike-Slip Linea On Europa

Marissa Elizabeth Cameron
University of Texas at El Paso, mecameron@miners.utep.edu

MODELING TIDALLY DRIVEN COULOMB FAILURE AT STRIKE-SLIP LINEA ON EUROPA

MARISSA ELIZABETH CAMERON

Department of Geological Sciences

APPROVED:

Bridget Smith-Konter, Ph.D., Chair

Aaron A. Velasco, Ph.D.

Eric A. Hagedorn, Ph.D.

Benjamin C. Flores, Ph.D.
Dean of the Graduate School

Imagination will often carry us to worlds that never were.

But without it we go nowhere.

~Carl Sagan

MODELING TIDALLY DRIVEN COULOMB FAILURE AT STRIKE-SLIP LINEA ON EUROPA

by

MARISSA ELIZABETH CAMERON, A.S., B.S.

THESIS

Presented to the Faculty of the Graduate School of

The University of Texas at El Paso

in Partial Fulfillment

of the Requirements

for the Degree of

MASTER OF SCIENCE

Department of Geological Science

THE UNIVERSITY OF TEXAS AT EL PASO

May 2014

Acknowledgements

It amazes me that regardless of having "wandered off the beaten path" more than once I still find myself exactly where I belong, and with a greater appreciation for the journey that has brought me here. While this may partly be due to luck, I know much of it is because of the wonderful support system I have in my family, friends, colleagues, and teachers.

To my family – thank you for your unwavering support and acceptance. I still remember the times I spent with my dad: rock collecting by day and stargazing by night. Even though she may not realize it, my mom taught me everything there is to know about time-management and efficiency, which has proven essential in graduate school! And to Carl, who has endured several meltdowns, and somehow not only stuck around, but still loves me. To my friends – so many people in the department have encouraged me simply by being my friend and supporting me. Be it commiserating over killer homework assignments, or cramming for exams. And I owe so much to my partner in crime and best friend, Sandra, who somehow always knows what I'm thinking and has provided me with countless hours of comedic relief.

I have been fortunate to have a number of excellent teachers and mentors throughout the years. Josh Villalobos, my geology teacher at El Paso Community College is the reason I chose geology as my major, and was the one who encouraged me to apply for undergraduate research at UTEP. Dr. Aaron A. Velasco, who took me on his team even though I had almost no previous experience. He taught me countless computer skills and was the first person to teach me to do research. I am also pleased to thank Dr. Eric A. Hagedorn for being on my committee and providing useful insight. Dr. Robert T. Pappalardo at JPL, who always manages to make time for me in his hectic schedule. He has opened so many doors for me and I feel incredibly lucky to be able to work with such an esteemed scientist.

And finally, my advisor and role model, Dr. Bridget Smith-Konter, who gave me the amazing opportunity to combine my love for space with my love for earth science, changing the course of my academic career and giving me the push I needed to get back on track. Her open door policy ensured I never got overwhelmed or stuck, at least not for *too* long. Somehow she manages to make everything seem so easy without ever making me feel foolish. And her dedication not only to work but also to her family has been inspiring.

Abstract

The surface of Europa is crosscut by a dense network of fractures and there are many candidate faults for studying past tectonic activity. To better understand the role of tidal stress sources and implications for faulting on Europa, we investigate the relationship between shear and normal stresses at four fault zones: Agenor Linea, Rhadamanthys Linea, Conamara Chaos (Agave/Asterius Linea), and Astypalaea Linea, offering a unique comparison of geological activity of fractures residing in geographically diverse locations of Europa. Assuming tidal diurnal and non-synchronous rotation (NSR) stresses are the primary mechanisms for strike-slip tectonism, here we investigate the mechanics of Coulomb shear failure on Europa. We consider a range of friction coefficients (μ_f = 0.2 - 0.6) and fault depths (0-6 km) to evaluate how the failure varies as a function of depth and its dependency on ice friction, geographic location, and fault geometry. Our results indicate that the conditions for failure are not met for any of the lineae subject to diurnal stresses only. Alternatively, models that include both diurnal and NSR stress readily generate shear and normal stress magnitudes that could give rise to shear failure. In general, failure seems to be confined to depths < 6 km for all four linea. Failure is easily activated and extends to depths ranging from 3-6 km on all four linea systems when a low coefficient of friction (μ_f = 0.2) is applied, but is generally limited to depths < 3 km when a high coefficient of friction (μ_f = 0.6) is applied. Based on these results, we infer that the conditions for shear failure are met along at least these four studied linea, and possibly others, on Europa when NSR is adopted as a driving stress mechanism.

Table of Contents

List of Figures

1. Introduction

Europa is the smallest of Jupiter's four Galilean moons, with a diameter of ~3100 km – similar to the size of Earth's Moon (~3400 km). Between 1995 and 2003, the space probe Galileo gathered data on the Jupiter system. Imagery from Galileo flybys reveal Europa's surface to be extensively fractured by linear features [*Greenberg et al.,* 1998]; high resolution images of the linear features on Europa's surface show what looks to be strike-slip offsets [*Schenk and McKinnon*, 1989; Prockter *et al.,* 2000; *Kattenhorn*, 2004], suggesting at least some of the features may have a transform type of faulting history. The lack of craters suggests that tectonic activity regenerates the surface. In December 2012, the Hubble Space Telescope detected water vapor above Europa's south polar region, providing strong evidence of water plumes erupting off the moon's surface [*Roth et al.,* 2013]. In addition, magnetic field data from Galileo provides evidence of an induced magnetic field, suggesting the presence of a subsurface liquid water ocean [*Ojakangas and Stevenson,* 1989; *Carr et al.,* 1998], which has unique implications for the evolution of Europa's tectonic history and stressing mechanisms. To gain a better insight into such global stress mechanisms acting on and within Europa throughout its tectonic history, a synthesized examination of surface morphology, the source of stresses on strike-slip lineaments, and failure dynamics responding to these stresses is required.

Here we examine fundamental questions about the role and evolution of strike-slip tectonism on Europa as it relates to the global stress field. Previous studies have suggested that diurnal tidal stresses (1) are responsible for the formation of Europa's ridges [*Greenberg et al.,* 1998; *Hoppa et al*., 1999; *Nimmo and Gaidos*, 2002], and (2) may trigger geological activity along fractures of other icy moons, like Enceladus and Ganymede [*Showman and Malhotra,* 1997; *Nimmo et al*., 2007; *Smith-Konter and Pappalardo,* 2008; *Olgin et al.,* 2011]. Our analysis builds upon this cumulative body of work to assess the roles of both tidal diurnal stresses and non-synchronous rotation (NSR) stresses, which may arise when a satellite's outer icy shell has decoupled from its interior [*Ojakangas and Stevenson,* 1989]. NSR may potentially provide a critical stress contribution for shear failure to be achieved at depth along four fault zones investigated in this study (Figure 1): Agenor Linea, Rhadamanthys Linea, Conamara Chaos (Agave/Asterius Lineae), and Astypalaea Linea.

Using a computational model based on the Coulomb failure criterion, we quantify the

relationship between the shear and normal stresses resulting from tidal deformation of the icy shell of Europa. In general, the Coulomb failure criterion is a measure of a fault's potential to store stress in the form of fault locking (when normal stress dominates), or to release stress as fault slip (when shear stress dominates). If shear stress magnitudes exceed the Coulomb failure criterion, shear failure occurs and is manifested as either right- or left-lateral displacements. Global stress mechanisms also affect failure, in that surface patterns of compressive and tensile stress shift throughout its orbit. Here we examine the faulting criterion that supports shear failure as a function of depth of faulting and the coefficient of friction as a means for better understanding Europa's tectonic history.

2. Surface Geology

Much of Europa's surface is crosscut by a dense network of fractures, thus there are many candidate faults for studying past tectonic activity. In this study we focus on four major fault zones (Figure 1): Agenor Linea, Rhadamanthys Linea, Conamara Chaos region (Agave/Asterius Lineae), and Astypalaea Linea.

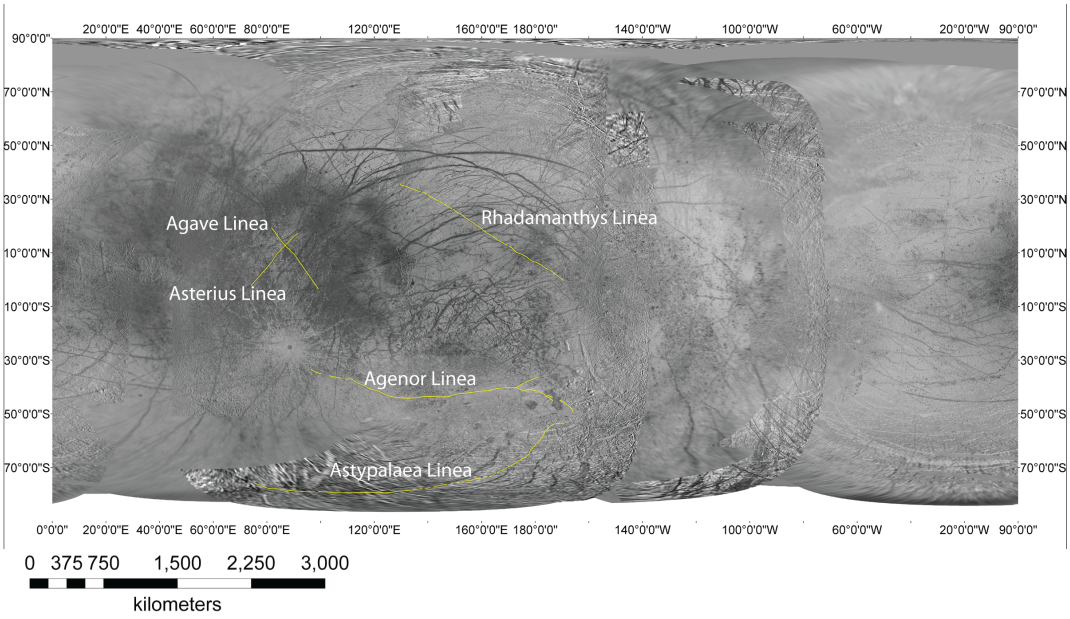

Figure 1: *Galileo* mosaic of Europa with target faults highlighted. Note: Astypalaea Linea shows the entire extent of the fault zone, while this study will focus only on individual fault segments. Image modified from *Prockter et al.*, (2000).

Agenor Linea is a unique bright band on Europa's surface, ranging from ~180° to 110° E from 37° to 44° S [*Prockter et al*., 2000], of ~1500 km in length. Agenor Linea has unusual photometric properties suggesting that it may have been active recently [*Geissler et al*., 1998]. However, high-resolution observations during Galileo orbit E17 show that it is crosscut by small fractures and mottled terrain, reducing the likelihood that it is currently active [*Prockter et al*., 2000]. *Voyager* analyses of Agenor Linea suggested a compressional origin [*Schenk and McKinnon*, 1989]. Alternatively, structural relationships within the fault band suggest that it formed by right-lateral strike-slip motion [*Prockter et al*., 2000], and additional analyses suggest additional structural associations [*Greenberg*, 2004; *Schenk et al*., 2007]. No features are observed to cut across it, suggesting in may be geologically young [*Schenk and McKinnon,* 1988].

Rhadamanthys Linea is generally a NW-SE oriented double ridge bright band spanning

Europa's northern mid-latitudes (35^{o} to 2^{o} N) and roughly the same longitudinal zone as Agenor Linea of ~1700 km in length. It has been characterized by a series of dark spots distributed along the central lineament, which may have formed due to intrusive and extrusive cryomagmatic processes [*Fagents et al.,* 2000]. Rhadamanthys Linea may have been a triple band in the early stages of formation based on its spectral characteristics and transitional morphology [*Belton et al.,* 1996]. Photogeologic evidence (this study) suggests a left-lateral sense of slip.

The Conamara Chaos region, in the mid to northern latitudes of Europa (35^{o} N to 15^{o} N), west of Rhadamanthys and Agenor Linea, is bordered by two prominent faults: Agave Linea (~2000 km in length) and Asterius Linea (~1400 km in length) [*Kattenhorn,* 2004]. These lineae are ridge-type strike-slip faults, or triple bands. Triple bands are prominent lineaments consisting of a bright central stripe flanked by broader dark margins. The average band width measurements are ~14 km for both lineae. There are instances of left-lateral slip along Agave Linea, though it has undergone only ~ 5 km of offset near Conamara Chaos [*Kattenhorn*, 2004]. Unfortunately, the entire length of Agave Linea was not captured in high-resolution Galileo images, so it is unknown if strike-slip offsets vary in other regions. Asterius Linea cross-cuts Agave Linea, making it the younger of the two, and displays evidence of right-lateral slip [ref].

Astypalaea Linea is composed of several discrete N-S striking, right lateral fault segments spanning Europa's high southern latitudes [*Prockter et al.,* 2009] ranging from 60°-79°S and 191°-268°W of ~810 km in total length. Like Agenor Linea, it is considered a band-like strike-slip fault, though unlike Agenor, the band-like appearance of Astypalaea likely resulted from dilation of the tailcracks, not dilation of the fault surfaces [*Kattenhorn*, 2004]. Astypalaea Linea has been documented in previous literature as a right-lateral fault with ~42 km of offset [*Tufts et al.,* 1999]. Astypalaea's surface is not heavily cratered, nor is it overprinted by many younger features, indicating it is geologically young.

3. Tidal Stress Mechanisms and Modeling

Global surface stresses arising from time variable tidal deformation have been used by many investigators to explain the pattern of observed fractured lineaments on the surface of Europa [e.g., *Helfenstein and Parmentier*, 1985; *McEwen*, 1986; *Leith and McKinnon*, 1996; *Geissler et al*., 1998; *Greenberg et al.*, 1998; *Hoppa*, 1998; *Hoppa et al.*, 1999; *Figueredo and Greeley*, 2000; *Kattenhorn*, 2002; *Spaun et al*., 2003; *Schenk et al*., 2007, *Rhoden et. al,* 2010]. Possible sources of tidal stress that have been associated with the formation of global tectonic features include reorientation relative to the spin axis [*Melosh*, 1975], tidal despinning [*Melosh*, 1977], radial and librational tides due to an eccentric orbit [*Yoder*, 1979; *Greenberg et al.*, 1998], non-synchronous rotation [*Helfenstein and Parmentier*, 1985], orbital recession and procession [*Squyres and Croft*, 1986; *Croft et al.* 1995], and polar wander [*Leith and McKinnon*, 1996; *Schenk et al*., 2007].

In this study, we limit our focus to two primary mechanisms of tidal deformation, diurnal and NSR stresses. As a tidally locked satellite orbits its parent planet, variations in gravitational tidal forces, due in part to the satellite's eccentric orbit, act to deform the moon's surface. These stresses vary over a period equal to that of the satellite's orbital (diurnal) period, or 3.55 days for Europa. As the satellite orbits, radial and librational tides combine to create a pattern of stresses that sweep across the surface. Previous studies have suggested that diurnal tidal stresses are responsible for the formation of Europa's ridges [*Greenberg et al*., 1998; *Hoppa et al*., 1999; *Nimmo and Gaidos*, 2002].

NSR stresses may arise if a tidally flexed satellite has an outer icy shell that is decoupled from its interior [*Helfenstein and Parmentier*, 1985]. As the outer shell rotates, the surface migrates eastward relative to the tidal bulge and can result in an additional source of stress within the viscoelastic icy shell. *Hoppa et al*. [1999] compared *Voyager* and *Galileo* observations to constrain the present NSR period of Europa's ice shell to be $> 10^4$ yr. It has also been suggested that the period of NSR stress may be on the order of the thermal diffusion timescale, or $\sim 10^7$ yr for Europa [*Ojakangas and Stevenson,* 1989; *Hoppa et al.,* 1999].

To investigate tidal diurnal and NSR stresses as a function of orbital position past periapse (i.e., the mean anomaly, m) and geographic location on the surface of Europa, we utilize SatStress, a numerical code that calculates tidal stresses at any point on the surface of a satellite.

SatStress computes stresses based on tidal potential theory [*Wahr*, 1981], allowing both elastic and layered Maxwell viscoelastic treatments of the lithosphere, and computes both raw ($\sigma_{\varphi\varphi}$, $\sigma_{\theta\theta}$, $\sigma_{\theta\varphi}$ or latitudinal, longitudinal, and shear stresses, respectively) (Figure 3-4) and diagonalized (principal) (Figure 2) stress tensor components. We adopt SatStress model parameters appropriate to a spherically symmetric ice shell of thickness 20 km, underlain by a global subsurface ocean: shear modulus μ = 3.5 GPa, Poisson ratio ν = 0.33, gravity g = 1.32 m/s^2, ice density r = 920 kg/m^3, satellite radius R = 1.56 x 10^3 km, satellite mass M = 4.8 x 10^{22} kg, semi-major axis a = 6.71 x 10^5 km, and eccentricity e = 0.0094. To investigate stresses arising from a diurnal stress model alone (assuming a negligible NSR period of 10^7 yr), we adopt elastic Love numbers h_2 = 1.2 and l_2 = 0.32 [*Wahr et al.,* 2009]. Alternatively, to simulate the diurnal + NSR tidal stress field, we adopt an NSR period of 1.422 x 10^5 yr from *Wahr et al.* [2009], using Love numbers of h_2 = 1.8 (real) and -4.2 x 10^{-3} (imaginary), and l_2 = 0.47 (real) and -2.8 x 10^{-3} (imaginary) [*Wahr et al.,* 2009].

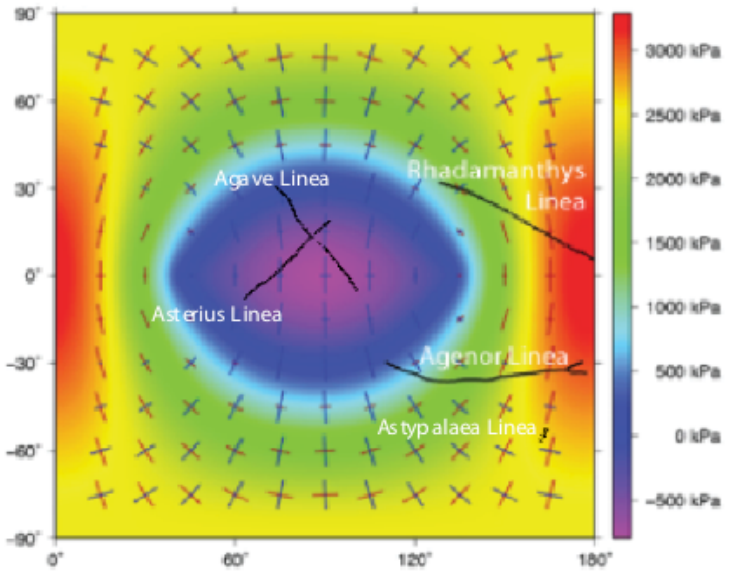

Figure 2: Maximum principal stress map for Europa at periapse (or mean anomaly position *m* = 0°) for a diurnal + NSR model. The fault zones are also labeled for reference. Positive values indicate stresses are in a tensile state, negative values indicate a compressive state.

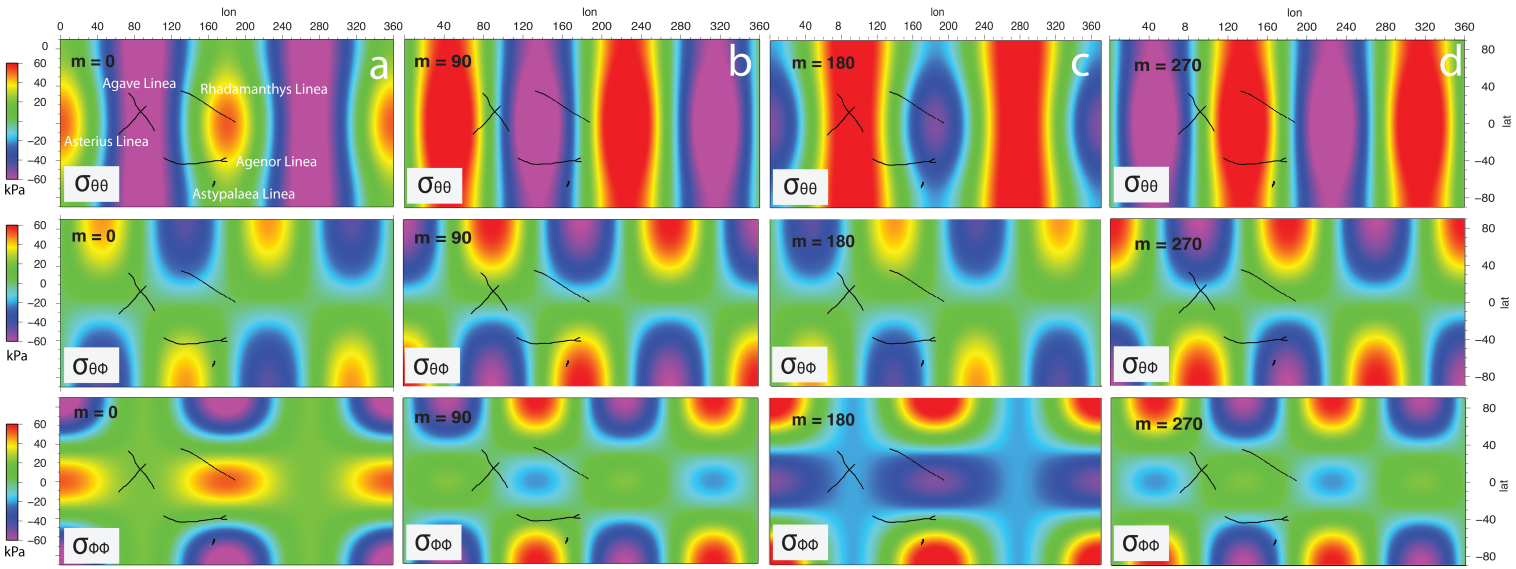

Figure 3a-3d: Global view raw stress tensor field calculated at mean anomaly, *m* = 0, 90, 180 and 270° for a diurnal only model. Note stress amplitudes are in kPa.

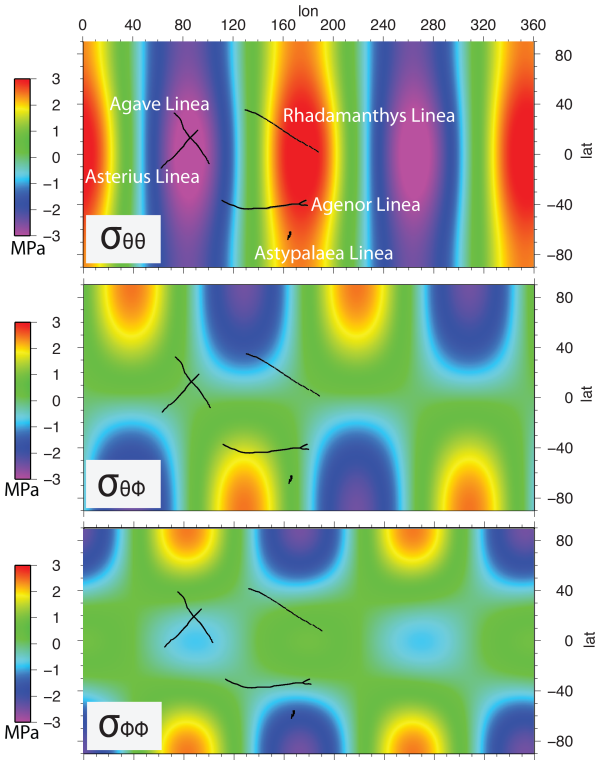

Figure 4: Global view of raw stress tensor fields at periapse (or mean anomaly position *m* = 0°) for a diurnal + NSR model. Note stress amplitudes are in MPa. This snapshot of the stress field is provided for *m* = 0° and is representative of all *m* positions, as stresses from this model only vary in magnitude by ~60 kPa over an orbital cycle.

To demonstrate the behavior of Europa's predicted principal tidal stresses as a function of orbital position, we first plot the maximum principal tensile stress for both diurnal only and diurnal + NSR models (Figure 2). Positive values indicate stresses are in a tensile state, negative values indicate a compressive state. Next, to illustrate diurnal stress variation as a function of mean anomaly, we plot the raw stress field at 90° intervals for the diurnal only model (Figure 3). The stress field at periapse is provided for the diurnal + NSR model (Figure 4). The diurnal model only shows that the most variation in stresses occurs with the $\sigma_{\theta\theta}$ (longitudinal) component, with all of the faults experiencing a peak stress of ~60 kPa at some point in Europa's orbit. The diurnal + NSR model shows that the all of Agave and Asterius Linear lie within zones of high negative stress (~-3 MPa), while eastern portion of Agenor and Rhadamanthys Linea lie within zones of high positive stress (~3 MPa), in the $\sigma_{\theta\theta}$ component.

4. Coulomb Failure

Following the methodology of previous studies [*Nimmo et al*., 2007; *Smith-Konter and Pappalardo*, 2008; *Olgin et al*., 2011], we resolve raw stress tensor components onto discrete fault segments of varying length and of varying orientation into both normal (σ_n) and shear (τ_s) stress components:

$$\tau_s = \frac{1}{2}\left(\sigma_{\phi\phi} - \sigma_{\theta\theta}\right)\sin 2\beta + \sigma_{\theta\phi}\cos 2\beta \qquad \text{(Eq. 1)}$$
$$\sigma_n = \sigma_{\theta\theta}\cos^2\beta + \sigma_{\phi\phi}\sin^2\beta + \sigma_{\theta\phi}\sin 2\beta$$

where β is the fault orientation, defined with respect to the longitudinal direction. Where applicable, we adopted mapped linea traces from previous studies; however, due to limited availability of high-resolution imagery, we conservatively digitized fault geometry in some regions. For each individual fault segment, the normal stress component is defined as that acting perpendicular to the fault plane, while the shear stress component is that acting parallel to the fault plane.

To investigate the interrelated roles of shear and normal stress, we employ the Coulomb failure criterion [*Byerlee*, 1978] to assess the failure potential of individual fault segments [i.e., *Smith-Konter and Pappalardo*, 2008; *Olgin et al.*, 2011]. This model balances stresses that encourage and resist the motion of a fault, simultaneously accounting for both normal and shear tidal stresses, the coefficient of friction of ice, and additional stress at depth due to the overburden pressure. In this model, tidal shear stresses drive strike-slip motions, while normal stresses control a fault's frictional resistance to failure. To model this behavior, we calculate Coulomb stress,

$$\tau_c = |\tau_s| - \mu_f(\sigma_n + \rho g z) \qquad \text{(Eq. 2)}$$

where τ_s and σ_n are the shear and normal stresses, $\rho g z$ is the overburden pressure (z is the vertical depth of the fault plane), and μ_f is the effective coefficient of friction. The sign of the overburden stress quantity is taken to be positive, while the normal tidal stress is assumed positive when in compression and negative when in tension. The sign of the shear stress (positive for right-lateral, negative for left-lateral) becomes important when inferring the direction of slip when the failure conditions are met. Compressive stresses work to clamp a fault together, thus enhancing the

frictional resistance and inhibiting failure, and require higher shear stresses to overcome the failure criterion. Alternatively, tensile stresses work to unclamp a fault, thus reducing the frictional contact between fault surfaces and encouraging failure if the acting shear stress is large enough. In general, the failure criterion is most easily met when tensile stresses dominate.

For simplicity, we will refer to the right side Eq. 1 as the "frictional stress." Thus, for shear failure to occur, the tidal shear stress on a fault must be greater than the frictional stress. According to this model, shear failure will occur on optimally oriented fault segments when the shear stress exceeds the frictional resistance of the fault. Negative Coulomb stresses imply a locked fault, while positive stresses imply conditions supporting fault slip in a shearing sense. Because the Coulomb criterion only applies for a closed fault interface, we evaluate the role of fault depth for both normal tensile and compression regimes separately. For compressive zones, no minimum fault depth limitation applies, as a fault interface will always be closed. For tensile zones, the overburden stress must be larger than the tensile stress (otherwise a fault would dilate).

In this study we consider a range of friction coefficients (μ_f = 0.2 - 0.6), consistent with laboratory estimates of ice friction [*Schulson and Fortt,* 2012]. We also evaluate the depth of faulting for each linea. We perform Coulomb failure calculations at 0.1 km discretized fault depth increments from the surface down to z = 6 km to evaluate how failure varies as a function of depth and its dependency on ice friction, geographic location, and fault geometry.

5. Results: Shear Failure Along Lineae

5.1 Diurnal Case

We first evaluate the opportunity for shear failure at each fault zone resulting from diurnal tidal stresses alone (Figure 5-8). In these figures, we use an example case to demonstrate the diurnal stress cycle at 90° increments in mean anomaly position for each linea, as observed at 1 km depth, assuming a low ($\mu_f = 0.2$) coefficient of friction. Compressive stresses dominate both Agenor Linea and Rhadamanthys Linea at $m = 90°$, while tensile stresses dominate at $m = 270°$. Agenor Linea experiences shear stresses that transition from right-lateral at periapse to left-lateral at apoapse. Alternatively, Rhadamanthys Linea experiences mostly left-lateral shear stresses at $m = 90°$, and transitions to right-lateral near $m = 270°$. At $m = 90°$ and $m = 270°$, the western sections of Agave and Asterius Linea are primarily dominated by tensile and then compressive stresses, respectively. Agave Linea is dominated by right-lateral shear stress at periapse and left-lateral shear stress at apoapse. Alternatively, Asterius Linea is dominated by left-lateral shear stress at periapse and right-lateral shear stress at apoapse. Compressive stresses act on Astypalaea Linea at periapse while tensile stresses dominate at apoapse. For $m = 0$ - $90°$, Astypalaea Linea experiences right-lateral shear stresses; for $m = 180$ - $270°$, Astypalaea Linea experiences left-lateral shear stresses.

In general, the conditions for Coulomb failure are not met for any of the lineae subject to only diurnal stresses (Figures 5-8, bottom panels) because the overburden magnitude is too great. We illustrate these results at 1 km depth (map view) for demonstrative purposes, however for depths on the order of 1 km and greater, shear failure from diurnal tidal stress mechanisms is difficult to achieve because the relatively large overburden stress (1.2 MPa at $z = 1$ km) dominates the stress field and thus Coulomb stress is always negative. At Agenor Linea (Figure 5), for example, peak shear and normal diurnal stress amplitudes (~35 kPa, ~70 kPa) cannot overcome the large overburden stress. These stresses are of similar magnitude for the other fault zones as well: Rhadamanthys Linea (~10 kPa, ~80 kPa), Conamara Chaos fault zone (~70 kPa, ~50 kPa), and Astypalaea Linea (~60 kPa, ~40 kPa). For reference, Jupiter-Europa tidal stresses are significantly higher than Earth-Moon tidal stresses, which range between only 1-4 kPa [*Melchior*, 1983]. Although the Jupiter-Europa stresses fluctuate on a diurnal timescale, the fluctuation is small (~ 60 kPa) in comparison to the magnitude of the overburden stress, which

remains constant. The remaining portion of the diurnal cycle produces nearly identical failure results for all linea, with negative Coulomb stress results and thus no opportunity for failure given even the smallest ($\mu_f = 0.2$) ice friction values tested. Because the occurrence of strike-slip fault motion would be expected on Europa given the satellite's many observed strike-slip offset features, we next consider the role of NSR stresses as a secular stress source for strike-slip faulting at Agenor Linea.

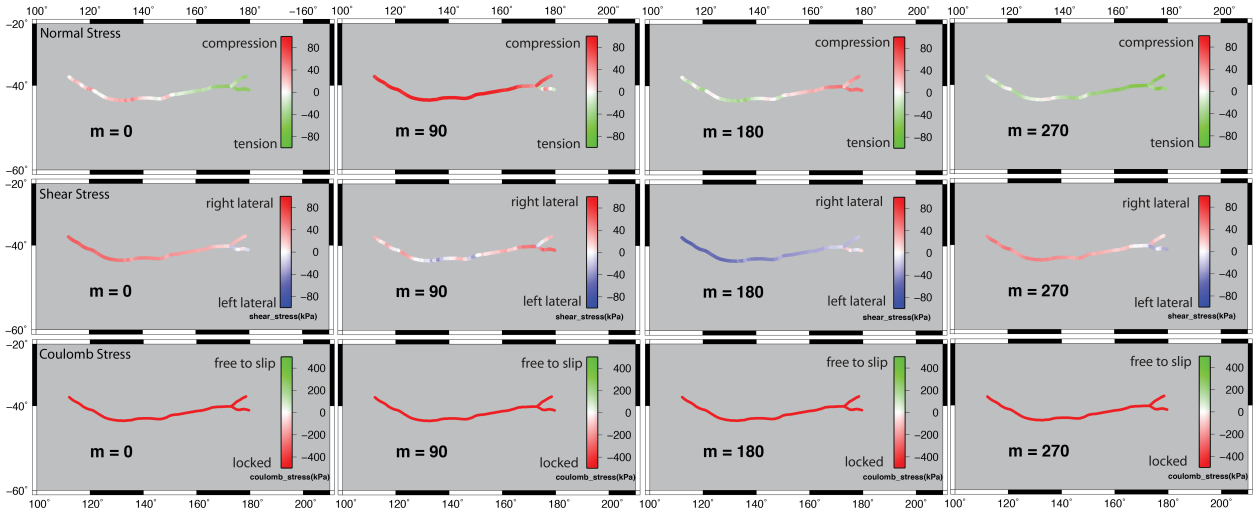

Figure 5: Diurnal normal, shear, and Coulomb stresses at Agenor Linea, calculated at mean anomaly m = 0, 90, 180, and 270°. For this model, stresses calculated at a depth of z = 1 km and assuming $\mu_f = 0.2$.

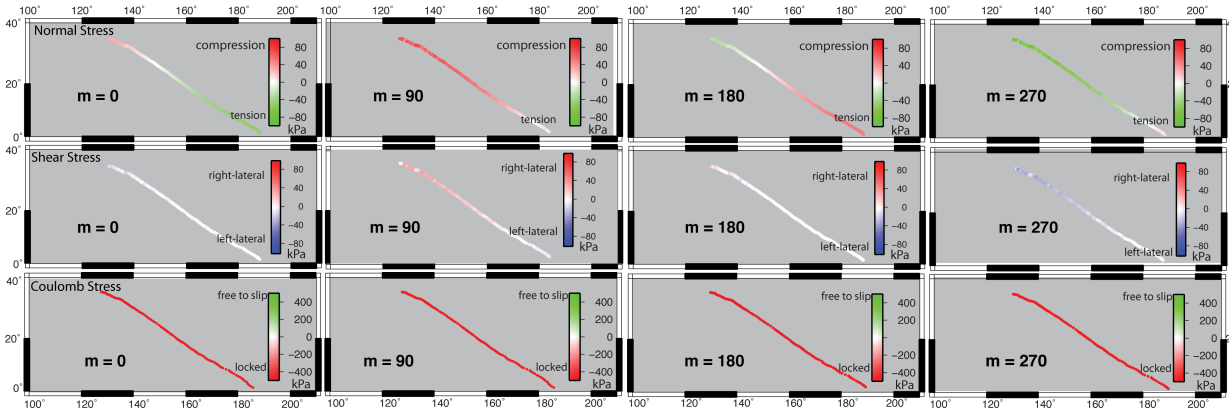

Figure 6: Diurnal normal, shear, and Coulomb stresses at Rhadamanthys Linea, calculated at mean anomaly m = 0, 90, 180, and 270°. For this model, stresses calculated at a depth of z = 1 km and assuming $\mu_f = 0.2$.

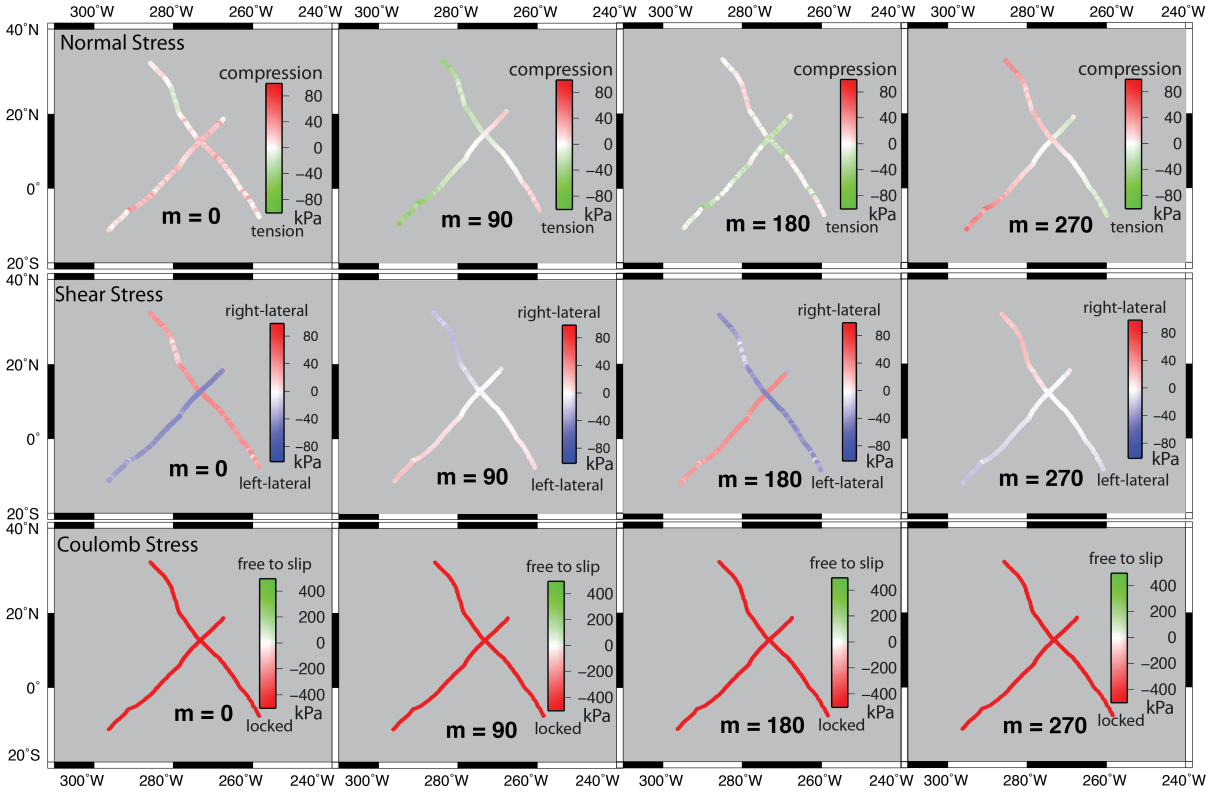

Figure 7: Diurnal normal, shear, and Coulomb stresses at Agave and Asterius Linea, calculated at mean anomaly m = 0, 90, 180, and 270°. For this model, stresses calculated at a depth of z = 1 km and assuming μ_f = 0.2.

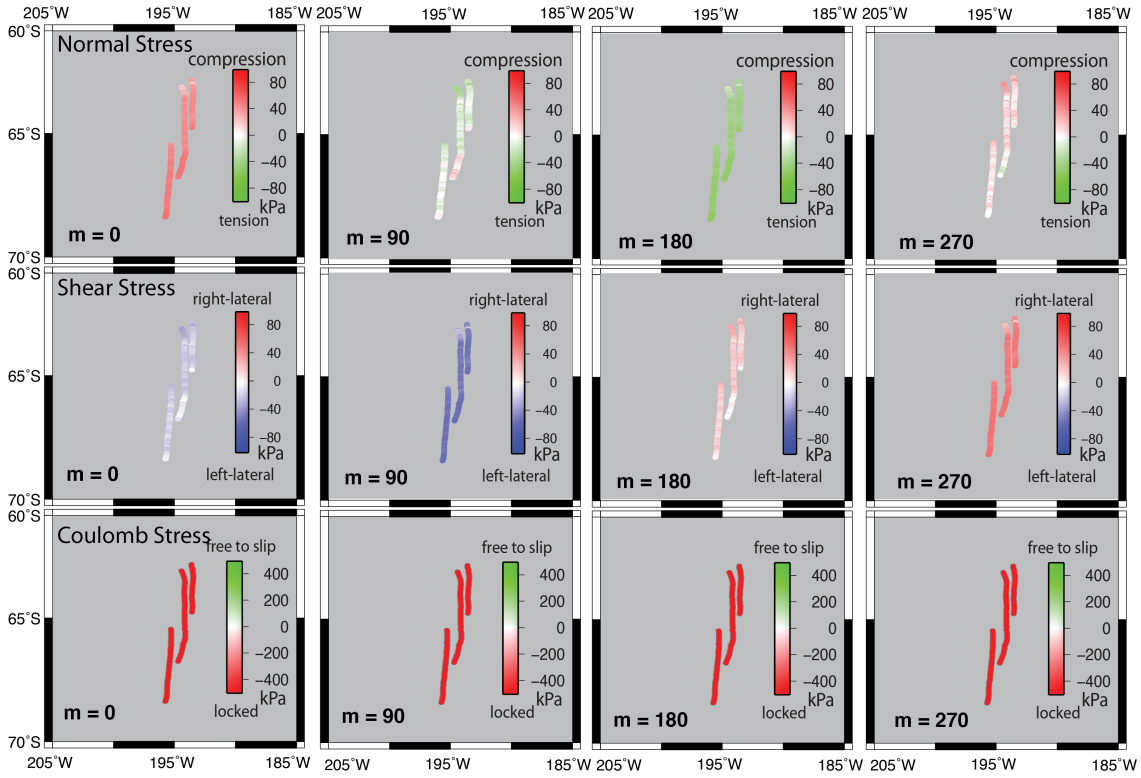

Figure 8: Diurnal normal, shear, and Coulomb stresses at Astypalaea Linea, calculated at mean anomaly m = 0, 90, 180, and 270°. For this model, stresses calculated at a depth of z = 1 km and assuming μ_f = 0.2.

5.2 Diurnal + NSR Case

NSR can provide stresses on the order of one to several MPa for ~1° of NSR as traditionally parameterized [*Greenberg et al*., 1998; *Leith and McKinnon*, 1996], or by steady-state rotation of a viscoelastic ice shell of viscosity ~10^{22} Pa s and rotation period ~ 10^{4} – 10^{5} yr in the SatStress parameterization [*Wahr et al*., 2009]. Assuming an NSR period of 1.422 x 10^{5} yr [*Wahr et al*., 2009] and other parameters fixed as above, we next investigate the conditions for shear failure resulting from a diurnal + NSR tidal stress model. Figures 9, 11, 13 and 15 illustrate these results in map view (m = 0°, z = 3 km, and μ_f = 0.2 and 0.6) for each linea. To evaluate the sensitivity of our models to both fault depth and ice friction, we also plot Coulomb failure for depths z = 0-6 km. A comparison of high friction (μ_f = 0.6) and low friction (μ_f = 0.2) as a function of depth is presented in Figures 10, 12,14, and 16.

For our Europa model, the resulting NSR stress amplitudes are a factor of 10 – 60 times larger than diurnal stress amplitudes, dominating the total stress magnitude over diurnal

timescales, with vary little failure variation. For example, peak shear and normal stress along Agenor Linea range from ~ 1.55 - 1.60 MPa and ~0.6 - 0.7 MPa, respectively, over the full diurnal cycle. Thus a snapshot of the stress at mean anomaly position $m = 0°$ is quite illustrative of the complete diurnal pattern. Because the Coulomb criterion only applies for a closed fault interface, we evaluate the role of fault depth for both normal tensile and compression regimes separately; this requirement limits Coulomb failure to depths greater than ~2 km (consistent with overburden stress of 2.4 MPa) for some tensile stress regimes along Agenor and Rhadamanthys, as tensile stress from diurnal + NSR contributions can be as high as ~ 3 MPa in some regions. Overall, these calculations demonstrate that both an increase in the coefficient of friction and fault depth result in a decrease in fault failure, which is limited to the upper few kilometers of the ice shell.

Agenor Linea: Along Agenor Linea, shear stresses are primarily right-lateral (~1.8 MPa), while normal stresses are predominantly compressive along the west side of the structure (~0.7 MPa) and tensile along the east side (~2.9 MPa). This along-fault dichotomy arises because of the large-scale variation in the regional stress field; Agenor Linea straddles a significant change in stress, for example, in the $\sigma_{\theta\theta}$ component, as is evident in Figure 4. It is interesting to note that the right-lateral shear stress direction implied by NSR is related to the fault's east-west orientation. If the fault were oriented in the north-south direction, NSR would generate only left-lateral shear and compressive normal stress, neither of which could constructively combine to produce right-lateral offsets like those observed at Agenor Linea [e.g., *Prockter et al*., 2000].

Applying the Coulomb criterion for depths ranging from 0.1 – 5 km, we find that all segments of Agenor Linea achieve shear failure over a limited depth range. For the low friction $\mu_f = 0.2$ model, at 0.1 – 2 km depth, only compressive zones are subject to failure, with patches of slip manifested along the west side of the fault. At 3 km depth, where the overburden is > 3.6 MPa, both compressive and tensile zones are subject to shear failure. Only the east side of the main branch transitions to a locked fault, while both the northern and southern branches that extend further eastward are still free to slip. For the high friction $\mu_f = 0.6$ model, at 0.1 – 2 km depth, again only compressive zones are subject to shear failure, with patches of slip manifested along the west side of the fault. At ~3 km depth, both compressive and tensile zones are subject to shear failure; however, Coulomb stresses suggest that the west side of the fault transitions to a

locked state, while large sections of the east side can achieve modest shear failure at deeper depths. For depths greater than 5 km, Coulomb stresses suggest a completely locked fault from end to end.

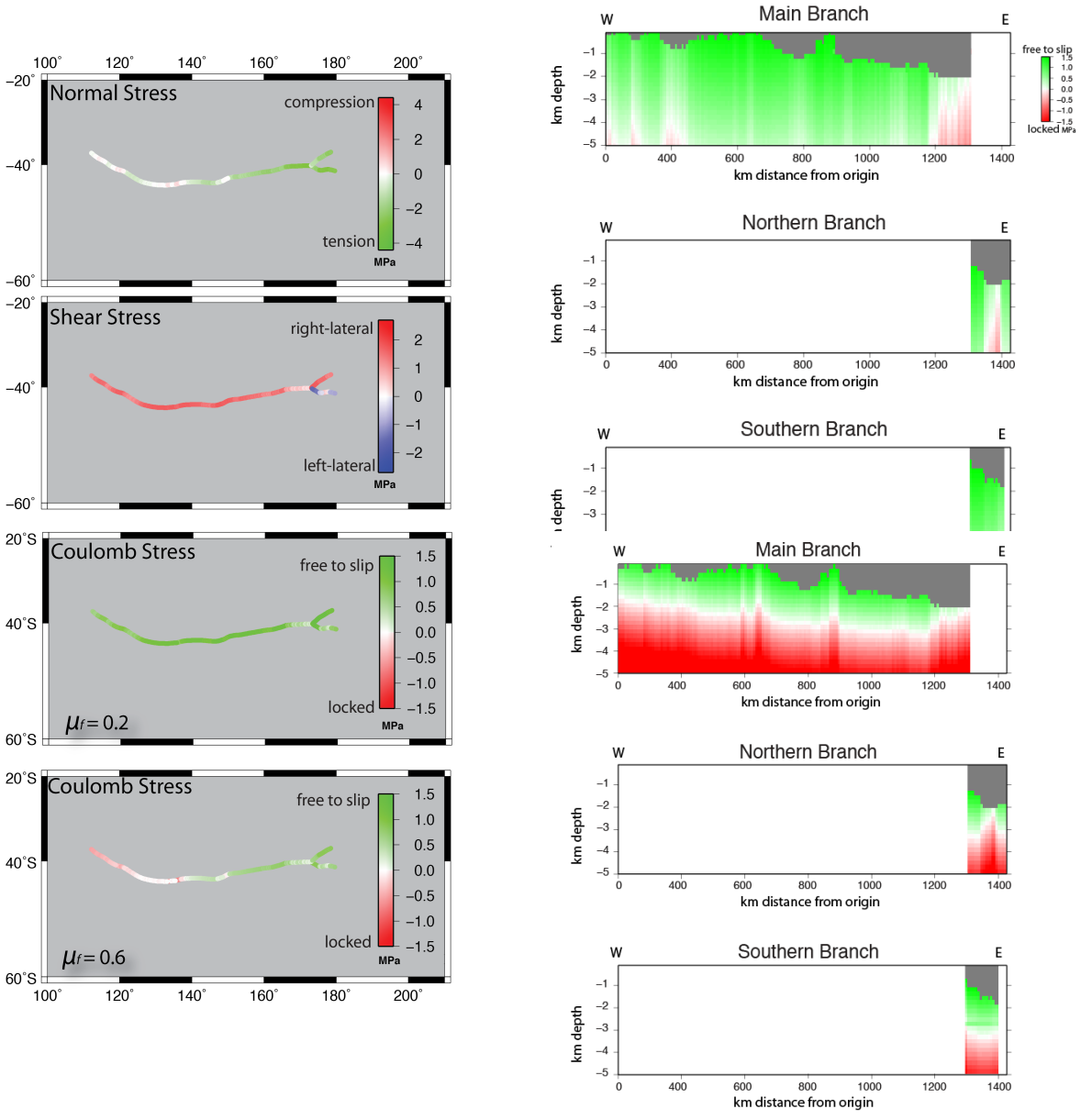

Figure 9 (left). Diurnal + NSR normal, shear, and Coulomb stresses at Agenor Linea, calculated at mean anomaly m = 0. For this model, stresses are illustrated at an example depth of z = 3 km and for μ_f =0.2 (low friction case) and 0.6 (high friction case). Figure 10 (right). Same as in Figure 10, but Coulomb stresses are now presented as a function of depth. Both low friction μ_f = 0.2 and high friction μ_f = 0.6 cases are provided. Gray segments represent shallow regions of high tensile stress not subject to Coulomb failure.

Rhadamanthys Linea: Along Rhadamanthys Linea (Figures 11-12), shear stresses from the diurnal + NSR model are left-lateral (~1.5 MPa), while normal stresses are predominantly compressive along the northwest side of the structure (~0.7 MPa) and tensile along the southeast side (~3 MPa). Like Agenor Linea, the along-fault dichotomy arises because of the large-scale variation in the regional stress field in the $\sigma_{\theta\theta}$ component (Figure 4). Applying the Coulomb criterion for appropriate depths ranging from 0.1 – 5 km, we find that all segments of Rhadamanthys Linea achieve shear failure over a variable depth range, depending on the coefficient of friction. For the low friction μ_f = 0.2 case, the model suggests at 0.1 – 2 km depth only compressive zones are subject to shear failure, with patches of slip manifested along the northwest side of the fault, again propagating eastward. With the small μ_f, failure is possible at significant depths, with the zone of depths < 4 km permitting shear failure throughout. Even at 5 km, Coulomb stresses indicate substantial fault activity, with small sections along the northwest side transitioning to a locked state. For the high friction μ_f = 0.6 model, at 0.1 – 2 km depth, only compressive zones are subject to shear failure, with patches of very shallow slip manifested along the northwest side of the fault and propagating eastward. At 3 km depth, Coulomb stresses suggest that the northwest side of the fault transitions to a locked state, while portions along the southeast side can achieve shear failure. For depths greater than 4 km, Coulomb stresses suggest a completely locked fault from end to end.

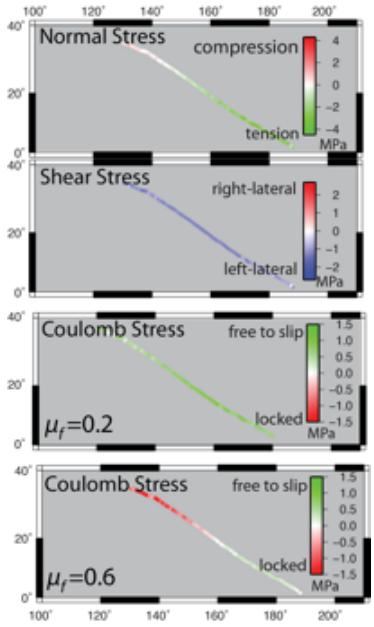

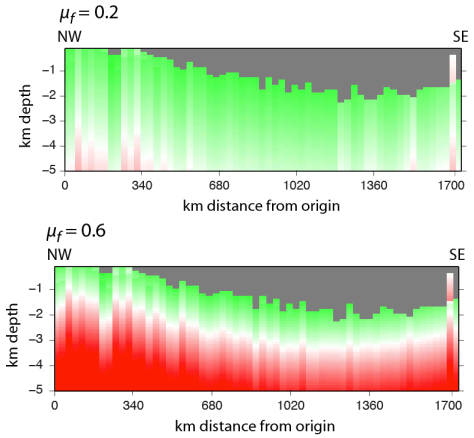

Figure 11 (left). Diurnal + NSR normal, shear, and Coulomb stresses at Rhadamanthys Linea, calculated at mean anomaly m = 0. For this model, stresses are illustrated at an example depth of z = 3 km and for μ_f =0.2 (low friction case) and 0.6 (high friction case).
Figure 12 (right). Same as in Figure 10, but Coulomb stresses are now presented as a function of depth. Both presented as a function function of depth. Both low friction μ_f = 0.2 function of depth. Both low friction μ_f = 0.2 and high friction μ_f = 0.6 cases are provided. Gray segments represent shallow regions of high tensile stress not subject to Coulomb failure.

Conamara Chaos fault zone: For this complex region, model predicts shear stresses that are primarily right-lateral (~1 MPa) along Agave Linea, and left-lateral (~1.2 MPa) along Asterius Linea, while normal stresses are entirely compressive along both (~1 MPa) when NSR is included (Figures 13-14). The opposite sense of slip between the two faults is a function of each linea's respective strike. We discuss this anomaly, and its relationship to offset observations, in further detail in Section 6. Assuming low friction (m_f = 0.2), failure can extend down to 3 km depth along both lineae, with a section along the west side of Agave Linea and the southernmost sections of both faults transitioning to a locked phase. The abrupt changes in locked and slipping zones alone both Agave and Asterius Linea are likely due to changes in *b* angles, which correspond to changes in strike. Assuming high friction (m_f = 0.6), failure is strictly limited to a small section on Agave Linea at 1 km depth. Failure is limited even further for Asterius Linea, with only the upper few 100s of meters supporting stresses indicative of shear failure.

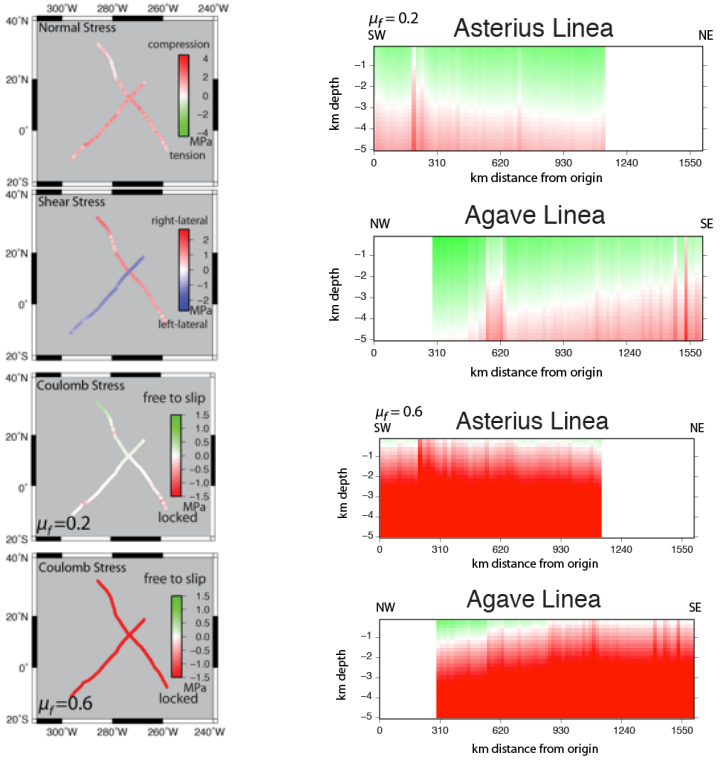

Figure 13 (left). Diurnal + NSR normal, shear, and Coulomb stresses at Agave and Asterius Linea, calculated at mean anomaly m = 0. For this model, stresses are illustrated at an example depth of z = 3 km and for μ_f =0.2 (low friction case) and 0.6 (high friction case). Figure 14 (right). Same as in Figure 10, but Coulomb stresses are now presented as a function of depth. Both low friction μ_f= 0.2 and high friction μ_f= 0.6 cases are provided. Gray segments represent shallow regions of high tensile stress not subject to Coulomb failure.

Astypalaea Linea: Shear stresses are primarily left-lateral (~1 MPa) along the fault segments of Astypalaea Linea (Figures 15-16), although a small southern section of the easternmost branch is right-lateral (~0.8 MPa). Normal stresses are entirely compressive along each segment (~1 MPa). Assuming low friction ($m_f = 0.2$), failure for this model can extend down to 4 km depth, however there is never a scenario where an entire segment fails. For the $\mu_f = 0.6$, failure is strictly limited to a small section at the north end at 1 km depth.

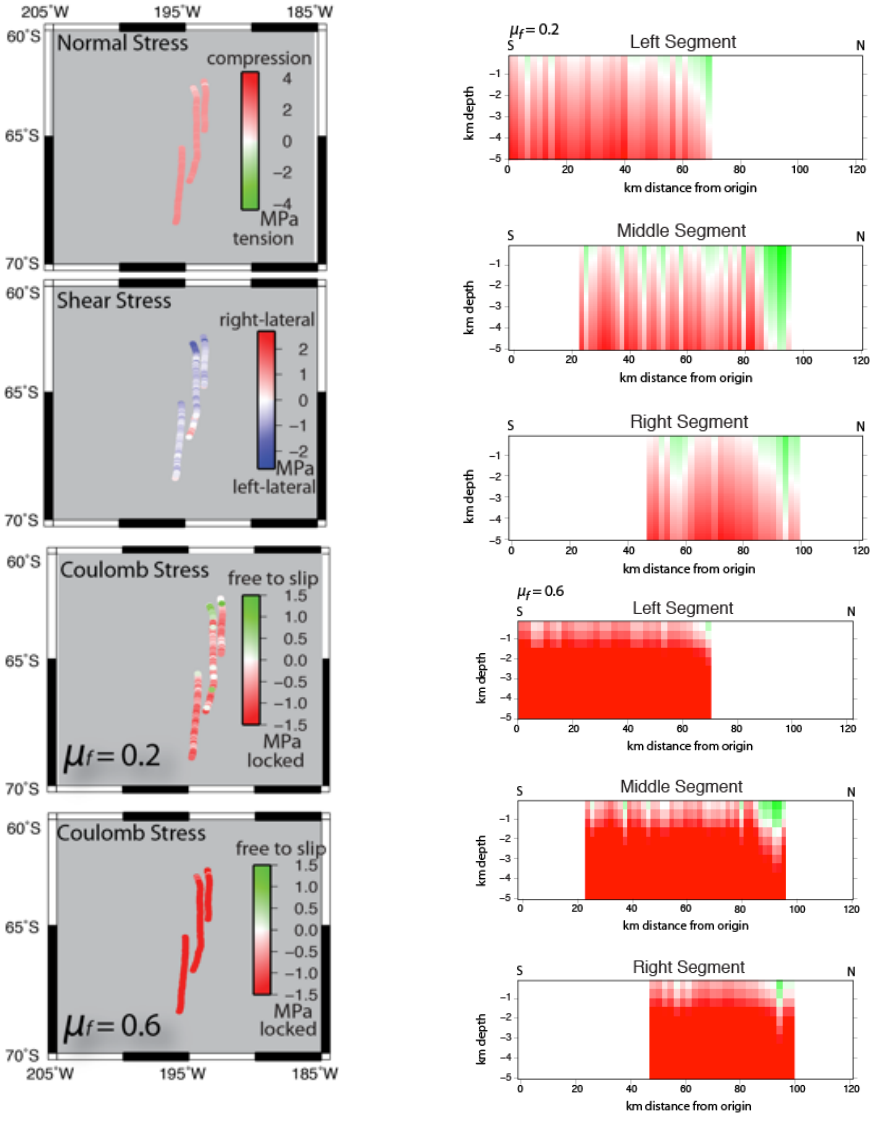

Figure 15 (left). Diurnal + NSR normal, shear, and Coulomb stresses at Astypalaea Linea, calculated at mean anomaly m = 0. For this model, stresses are illustrated at an example depth of z = 3 km and for μ_f =0.2 (low friction case) and 0.6 (high friction case). Figure 16 (right). Same as in Figure 10, but Coulomb stresses are now presented as a function of depth. Both low friction μ_f = 0.2 and high friction μ_f = 0.6 cases are provided. Gray segments represent shallow regions of high tensile stress not subject to Coulomb failure.

6. Discussion

6.1 Failure depth and friction constraints

Based on these results, we infer that shear failure is possible along at least these four studied fault systems spanning a major portion of Europa when NSR is included as a driving stress mechanism. In general, given the parameters investigated by this work, failure seems to be confined to depths < 6 km for all four linea, suggesting that there is a mechanical link to the brittle-ductile depth of Europa's icy shell, which has been estimated to be ~ 6 km. In comparison to nominal failure depths identified for Enceladus's tiger stripe fractures (< 3 km) [*Smith-Konter and Pappalardo*, 2008; *Olgin et al.*, 2011], fault depths on Europa, assuming a minimum coefficient of friction of 0.2, tend to be deeper and stronger. Preliminary work on Ganymede [*Cameron et al*., 2012] also suggests that fractured regions like Dardanus Sulcus, when subject to NSR stresses, may experience Coulomb failure limited to fairly shallow fault depths (< 2 km).

The San Andreas Fault System in California can be used as a terrestrial analog for evaluating failure depth limitations on Europa [*Tufts et al*., 1999], since it is also a strike-slip fault and is of a similar length (~1300 km) to many of the prominent lineae. Based on geodetic and seismological constraints, the San Andreas is known to have fault sections that are shallowly locked (2-5 km) [*Smith-Konter et al.,* 2011], linked to a high Coulomb stress accumulation rates [*Smith-Konter and Sandwell,* 2009]. These sections may also be accompanied by patches of near-surface (< 1 km) creep. It is also common for sections of the San Andreas fault to accommodate fault locking throughout the earthquake cycle at depths exceeding 6 km, although these sections accumulate Coulomb stress at slower rates. Along-strike fault depth variations of the San Andreas fault are not fully understood, however previous work has suggested these may be due to variations in strike geometry, lithology, and heat flow [e.g., *Miller and Furlong*, 1988; *Blackwell and Steele*, 1992; *Magistrale*, 2002; *Fuis et al*., 2007]. While this study investigates the role of tidal stresses on the depth of failure for linea of Europa, it is certainly possible that the driving rheological factors for fault depth variation on Earth play a key role in advancing (or terminating) fault failure and evolution on Europa.

To evaluate the sensitivity of our model to ice friction, we tested a suite of models representing frictional coefficients μ_f = 0.2 – 0.6 and presented the end-member results here. These results demonstrate how an increase in the coefficient of friction will result in a decreased

opportunity for fault failure. Failure is easily activated and extends to depths ranging from 3-6 km on all four linea systems when a low coefficient of friction is applied, but is limited to depths < 3 km (and even not feasible for some cases in the Conamara Chaos region) when a high coefficient of friction is applied. Laboratory experiments of ice motion validate ranges of $\mu_f = 0.1 – 0.7$ depending on sliding velocity, pressure, and temperature [*Beeman et al.,* 1988; *Fortt and Schulson*, 2007; *Schulson and Fortt,* 2012]. Previous studies have assumed a coefficient of friction appropriate to ice approaching its melting temperature ($\mu_f = 0.1$-0.3) for shear heating models on Europa and Enceladus [e.g., *Nimmo and Gaidos*, 2002; *Nimmo et al*., 2007; *Olgin et al*., 2011]. Indeed, our models suggest that low frictional coefficients are necessary for large-scale shear failure to occur throughout the fault zones; however, we have also shown that shear failure subject to high friction ($\mu_f = 0.6$) is feasible given the model parameters adopted for this study.

6.2 Slip predictions and observed offsets

Satellite imagery of Agenor Linea shows right-lateral offset in several locations with offsets of ~30 km [*Prockter et al*., 2009]. Our model predicts right-lateral slip for Agenor Linea. Photogeologic evidence of Rhadamanthys Linea suggests left-lateral offset (this study), which our model also predicts. *Hoppa et al*. [2000] report that observed displacement along Asterius Linea is right-lateral, while the upper left portion of Agave is left-lateral, but right-lateral to the southeast of Conamara Chaos. While our diurnal model predicts a cyclic behavior of right- and left- lateral shearing, Coulomb shear failure at depth is not likely to occur on diurnal timescales because of the significant overburden stress. Furthermore, our NSR model suggests a different slip sense than observed for both Agave and Asterius Lineae, perhaps implying alternate mechanisms (i.e., true polar wander or obliquity) could be the primary mechanism for failure rather than NSR. *Hoppa et al*. [2000] suggest that their sense-of-slip observations are likely associated with regional extension on the northeast and compression on the southeast sides of Conamara Chaos, although there is no evidence to support extension on the northeast side. A possible global compressional sink on the southeast side of Conamara Chaos has been suggested by *Greenberg et al.* [1999] to explain how the chaotic terrain may compensate for crustal extension at numerous dilation sites [*Tufts et al.*, 2000]. The presence of possible strike-slip

features and the apparent truncation of various lineaments by Astypalaea Linea suggest that fault displacement might have occurred, with 42 km of offset observed near Cyclades Macula, however examination of displaced features suggest at least 56 km of right-lateral offset [*Tufts et al.,* 1998; *Kattenhorn,* 2004].

Several groups have studied global slip predictions for Europa. *Hoppa et al.* [1999, 2000] used the tidal walking model to create global predictions of slip direction, which generally match the observed global pattern on Europa. *Rhoden et al*. [2011] made a correction to the predictions, but this did not affect the resulting global pattern of only left-lateral faults poleward of 35°N, only right-lateral faults poleward of 35°S, and between these regions, either right or left lateral faults depending on the longitude and the azimuth of the fault. The dominant orientations of observed lineae, NE and NW, are best fit if they formed in shear in response to nonsynchronous rotation stresses, potentially as modulated by diurnal stresses [*Spaun et al.,* 2003].

Deviations from global slip predictions may be due to a number of mechanisms that could alter fault location and/or orientation over time. As is evident from Figure 4 and 9-16, fault location and orientation (both large-scale orientation and local strike) will significantly impact the sense of slip. *Rhoden et al.* [2011] investigated the effects of obliquity on global stress predictions and concluded that an obliquity of ~1° could lead to offsets of the regions of mixed right and left lateral faults that are more consistent with the observations than polar wander. Gravitational interactions between Jupiter's largest satellites cause Europa's obliquity to be at least 0.1° and possibly larger if the satellite has a subsurface ocean [*Bills et al*., 2009]. Bow-shaped features, or cycloids, provide evidence of ~1° of obliquity [*Hurford et al*., 2009a]. *Rhoden et al*. [2010] found that good fits to cycloids were achieved only when longitude translation was assumed, for example, from an NSR influence, although cycloid fits did not suggest NSR as a source of formation.

Alternatively, true polar wander (TPW) involves reorientation of Europa's floating outer ice shell about the tidal axis with Jupiter. TPW is possible if the icy shell is latitudinally variable in thickness and decoupled from the rocky interior imposing high stress levels on the shell, up to an order of magnitude (or more) larger than diurnal tidal stresses [*Schenk et al.,* 2008]. It has been proposed as a possible explanation for some of the features whose tectonic patterns and stress history remains unexplained. Although Galileo imaging prevents global mapping of small-scale

features, it is believed that strike-slip fault distributions may be related to TPW with close to a 90° reorientation of the ice shell predicted. However, *Rhoden et al.* [2011] applied a slow polar wander model in an effort to explain the latitudinal mismatch between strike-slip predictions and observations, and found polar wander is no longer necessary once the effects of obliquity are included.

7. Conclusions

In this study we applied the Coulomb failure criterion to four fault zones of interest in an effort to gain a better insight into global stress mechanisms acting on Europa. Diurnal tidal deformation cannot provide large magnitude stress on the order of overburden stress, while NSR tidal deformation provides stresses ~1 to several MPa, depending on the assumed NSR rotation period. Using a NSR stress model, shear failure along the target features is possible although very sensitive to fault depth.

No Coulomb failure occurs for the diurnal stress models at any position, regardless of faulting depth or friction value, for any of these fault systems. Assuming stress contributions from NSR, shear failure along all lineaments examined is possible, although it is very sensitive to fault depth and m_f. For a low friction (m_f = 0.2), both Agenor Linea and Rhadamanthys Linea experience failure beyond 5 km, while the majority of both Agave and Asterius Linea are free to slip to ~3 km. For a high friction (m_f = 0.6), both Agenor Linea and Rhadamanthys Linea experience failure to ~2.5 km, while Agave and Asterius Linea are only free to slip to at depths < 1 km. Photogeologic evidence supports the sense of slip predicted by our model along Agenor and Rhadamanthys Linea, however does not for Agave and Asterius Linea, which may be due to alternate global stress mechanisms (i.e., true polar wander or obliquity changes). This is an issue that will be examined in future work.

8. Future Work

We will continue to identify alternate explanations of the differences in sense of slip between features, for example, Agave and Asterius Linea. Shallower depths (<1 km) will be examined for all features for a diurnal only case for consistency. Finally, a more extensive digitizing procedure will be applied to Astypalaea Linea. Specifically, we will examine the E-W trending trough feature that spans the high southern latitudes, rather than the N-S oriented fault segments presented here. Expanding the study region of Astypalaea Linea will likely provide more insight into the regions tectonic history.

Additional focus: Ganymede

The icy fractured surface of Ganymede also offers many candidate faults for studying both past and potentially present tectonic activity. Strike-slip tectonics appears to be common, and may be important to the development of Ganymede's surface, for example the transition from dark to light terrain [*Pappalardo and DeRemer*, 2003]. Preliminary work suggests that Ganymede may be subject to both diurnal and non-synchronous rotation (NSR) stresses, and under certain circumstances, these stresses can be sufficient to induce shear failure and produce strike-slip offsets, as inferred from Voyager and Galileo images [*Pappalardo and DeRemer*, 2003]. It is also possible that a past episode of high orbital eccentricity may have been crucial in the development of Ganymede's tectonic history [*Showman and Malhotra,* 1997]. Although not the primary focus of this thesis project, mapping and modeling will also be conducted on Ganymede features concurrently with Europa in order to better understand mechanisms of failure on icy satellites. Specifically, results from these tasks will address fundamental questions about the role and evolution of strike-slip tectonism on Ganymede and Europa, which will be the focus of M. Cameron's Ph.D. research.

References

Beeman, M., W. B. Dirham, and S.H. Kirby (1998), Friction of ice, *J. Geophys. Res*, 93, doi:10.1029/JB093iB07p07625.

Belton, M. J., J.W. Head, A.P. Ingersoll, R. Greeley, A.S. McEwen, K.P. Klaasen, … West, R.A. (1996), Galileo's first images of Jupiter and the Galilean Satellites, *Science* 274, 377–385.

Blackwell, D. D., and J. L. Steele (1992), The decade of North American geology, geothermal map of North America, scale 1:5,000,000, Geol. Soc. of Am., Denver.

Byerlee, J. D. (1978), Friction of rocks, *Pure Applied Geophysics*, 116, 615-626.

Carr, M. H., M. J. Belton, C. R. Chapman, M.E. Davies, P. Geissler, R. Greenberg, ... Veverka, J. (1998), Evidence for a subsurface ocean on Europa. *Nature*, 391, 363-365.

Croft, S.K., J.S. Kargel, R.L Kirk, J.M Moore, P.M. Schenk, R.G. Strom (1995), The geology of Triton. *Neptune and Triton*, University of Arizona Press, Tucson, pp. 879–947.

Fagents, S.A., R. Greeley, R.J. Sullivan, R.T. Pappalardo, L.M. Prockter (2000), Cryomagmatic mechanisms for the formation of Rhadamanthys Linea, triple band margins, and other low albedo features on Europa, *Icarus*, 144, 54-88.

Fortt, A.L. and E.M. Schulson (2007), The resistance to sliding along Coulombic shear faults in ice, *Acta Materialia,* 55, 2253-2264.

Fuis, G. (2007), The San Andreas fault in Southern California is almost nowhere vertical–Implications for tectonics, paper presented at the Annual Meeting of the Geological Society of America, Denver.

Greenberg, R., P. Geissler, G. Hoppa, B. R. Tufts, D. D. Durda, R. Pappalardo, J. W. Head, R. Greeley, R. Sullivan, M. H. Carr (1998), Tectonic processes on Europa: Tidal stresses, mechanical response and visible features, *Icarus*, 135, 64-78.

Greenberg, R. (2004), The evil twin of Agenor: Tectonic convergence on Europa, *Icarus*, 167, 313-319.

Helfenstein, P. and E. M. Parmentier (1985), Patterns of fracture and tidal stresses due to nonsynchronous rotation: Implications for fracturing on Europa, *Icarus*, 61, 175-184.

Hoppa, G., B.R. Tufts, R. Greenberg, P. Geissler (1999), Strike-slip faults on Europa: Global shear patterns driven by tidal stress, *Icarus*, 141, 287-298.

Hurford, T.A., A.R. Sarid, R. Greenberg, B.G. Bills (2009), The influence of obliquity on europan cycloid formation, *Icarus,* 202, 197-215.

Kattenhorn, S.A. (2004), Strike-slip fault evolution on Europa: Evidence from tailcrack geometries, *Icarus*, 172, 582-602.

Leith, A.C. and W.B McKinnon (1996), Is there evidence for polar wander on Europa?, *Icarus*, 120, 387-398.

Magistrale, H. (2002), Relative contributions of crustal temperature and composition to controlling the depth of earthquakes in Southern California, *Geophys. Res. Lett*., 29(10), 1447, doi:10.1029/2001GL014375.

Melchior, P. (1978*), The tides of the planet Earth*, 641, Pergamon, New York,

Melosh, H.J. (1975), Large impact craters and the Moon's orientation, *Sci. Lett*. 26, 353–360.

Melosh, H.J. (1977), Global tectonics of a despun planet, *Icarus*, 31, 221–243.

Miller, C. K. and K. P. Furlong (1988), Thermal-mechanical controls on seismicity depth distributions in the San Andreas Fault Zone, *Geophys. Res. Lett*., 15, 1429–1432, doi:10.1029/GL015i012p01429.

Nimmo, F. and E. Gaidos (2002), Strike-slip motion and double ridge formation on Europa, *J. Geophys. Res*., 107, doi:10.1029/2000JE001476.

Nimmo, F., J.R. Spencer, R.T. Pappalardo, and M.E. Mullen (2007), Shear heating as the origin of the plumes and heat flux on Enceladus, *Nature*, 447, 289-291.

Ojakangas, G.W. and D.J. Stevenson (1989), Thermal state of an ice shell on Europa, *Icarus*, 81, 220-241.

Olgin, J., B. Smith-Konter, R.T. Pappalardo (2011), The limits of Enceladus's ice shell thickness from tidally driven tiger stripe failure, *Geophys. Res. Lett*, 38, doi:10.1029/2010GL044950.

Prockter, L.M. and G.W. Patterson (2009), Morphology and evolution of Europa's ridges and bands, in *Europa*, edited by R. T. Pappalardo, W. B. McKinnon, and K. K. Khurana, pp. 237–258, Univ. Ariz. Press, Tucson.

Prockter, L. M., R.T. Pappalardo, and J.W. Head (2000), Strike-slip duplexing on Jupiter's icy moon Europa, *J. Geophys. Res*., 105, 9483-9488.

Rhoden, A.R., B. Militzer, E.M. Huff, T.A. Hurford, M. Manga, and M.A. Richards (2010), Constraints on Europa's rotational dynamics from modeling of tidally-driven fractures, *Icarus*, 210, 770-784.

Rhoden, A.R., T.A. Hurford, and M. Manga (2010), Strike-slip fault patterns on Europa: Obliquity or polar wander?, *Icarus*, 211, 636-647.

Roth, L., J. Saur, K.D. Retherford, D.F. Strobel, P.D. Feldman, M.A. McGrath and F. Nimmo (2013), Transient water vapor at Europa's South Pole, *Science,* 343, 6167, 171-174.

Schenk, P. and W.B. McKinnon (1989), Fault offsets and lateral crustal movement on Europa: Evidence for a mobile ice shell, *Icarus*, 79, 75-100.

Schenk, P., I. Matsuyama, and F. Nimmo (2008), True polar wander on Europa from global-scale small-circle depressions, *Nature,* 453, 368-371.

Schulson, E.M. and A.L. Fortt (2012), Friction of ice on ice, *J. Geophys. Res.,* 117, B12204, doi:10.1029/2012JB009219.

Showman, A. P. and R. Malhotra (1997), Tidal evolution into the Laplace resonance and the resurfacing of Ganymede, *Icarus*, 127, 93-111.

Smith-Konter, B. and R.T. Pappalardo (2008), Tidally driven stress accumulation and shear failure of Enceladus's tiger stripes, *Icarus*, 198, doi:10.1016/j.icarus.2008.07.005.

Smith-Konter, B. and D.T. Sandwell (2009), Stress evolution of the San Andreas Fault System: Recurrence interval versus locking depth, *Geophys. Res. Lett.*, 36, doi:10.1029/2009GL037235.

Smith-Konter, B., D. Sandwell, and P. Shearer (2011), Locking depths estimated from geodesy and seismology along the San Andreas Fault System: Implications for seismic moment release, *J. Geophys. Res*., 116, B06401, doi:10.1029/2010JB008117.

Spaun, N.A., R. T. Pappalardo, and J. W. Head (2003), Evidence for shear failure in forming near-equatorial lineae on Europa*, J. Geophys. Res*.,108, 5060, doi:10.1029/2001JE001499.

Squyres, S.W. and S.K. Croft (1986), The tectonics of icy satellites, in *Satellites,* edited by J. A. Burns and M. S. Matthews, pp. 293–341, Univ. Ariz. Press, Tucson.

Tufts, B. R., R. Greenberg, G. Hoppa, P. Geissler (1999), Astypalaea Linea: A large-scale strike-slip fault on Europa, *Icarus,* 141, 53–64.

Wahr, J. (1981). Body tides on an elliptical, rotating, elastic and oceanless Earth, *Geophys. J.R. Astr. Soc.*, 64, 677-704.

Wahr, J., Z.A. Selvans, M.E. Mullen, A.C. Barr, G.C. Collins, M.M. Selvans, R.T. Pappalardo (2009), Modeling stresses on satellites due to non-synchronous rotation and orbital eccentricity using gravitational potential theory, *Icarus*. 200, doi:10.1016/j.icarus.2008.11.002.

Vita

Marissa Cameron was born in California, and moved to El Paso, Texas as a child. She initially attended the University of Texas at El Paso as a Pre-Med Biology student. After transferring to El Paso Community College, she completed her coursework for Associate of Science degrees in both Geology and General Studies in 2010. She transferred back to UTEP to receive her Bachelor's in Geology in May 2012. During the summer of 2013, she was a research associate at NASA Ames in California as part of the 2013 NASA Ames Academy for Space Exploration. She will receive her Master of Science in Geophysics in May 2014, and will serve as the graduate student Marshal for the College of Science.

Permanent address: 12251 Russolo
El Paso, TX, 79936

This thesis was typed by Marissa E. Cameron.